Flow under Curvature: Singularity Formation, Minimal Surfaces, and Geodesics

David L. Chopp and James A. Sethian

CONTENTS

Chopp was supported in part by the National Science Foundation under grant CTS-9021021. A portion of his work was completed at the University of California, Los Angeles.

Sethian was supported in part by the Applied Mathematics Subprogram of the Office of Energy Research under contract DE-AC03-76SF00098, and the National Science Foundation and DARPA under grant DMS-8919074.

We study hypersurfaces moving under flow that depends on the mean curvature. The approach is based on a numerical technique that embeds the evolving hypersurface as the zero level set of a family of evolving surfaces. In this setting, the resulting partial differential equation for the motion of the level set function may be solved by using numerical techniques borrowed from hyperbolic conservation laws.

This technique is applied to several problems: the evolution of a dumbbell, and related many-armed surfaces, collapsing under mean curvature; the construction of a minimal surface attached to a given one-dimensional wire frame in $\mathbb{R}^3$, and, more generally, the construction of surfaces whose mean curvature is a prescribed function of position; the motion of curves on two-manifolds under flow that depends on geodesic curvature.

Some experiments involving flow controlled by Gaussian curvature are also included.

1. INTRODUCTION

We study the motion of hypersurfaces under flow that depends on the mean curvature. The main tool is a numerical technique, introduced in [Osher and Sethian 1988] and reviewed in Section 2, that follows the evolving hypersurface by regarding it as the zero level set of a time-dependent function. The resulting partial differential equations for the motion of the level set function may be solved by using numerical techniques borrowed from hyperbolic conservation laws. The advantage of this approach is that sharp corners and cusps are accurately tracked, and topological changes in the evolving hypersurface are handled naturally with no special attention.

1058-6458/96 $0.50 per page

Starting from this "level set approach" to propagating interfaces, this paper extends the technology in several directions. In Section 3.1 we study the collapse of a surface under motion by mean curvature. In [Sethian 1989] it was shown experimentally that the handle of a dumbbell pinches off, splitting the dumbbell into two surfaces, each of which collapses to a point. Here we show that an extension of this problem produces an interesting result: a multi-armed dumbbell leaves a separate, residual closed object at the center after the singularity forms. We verify this by studying a series of similar numerical problems, each showing this detached surface. In Section 3.2 we briefly consider flow under Gaussian curvature.

In Section 4 we use the level set approach to generate minimal surfaces attached to a given one-dimensional closed curve (wire frame) in $\mathbb{R}^3$. We construct a surface passing through the given curve and view it as the zero level set of a higher-dimensional function. We then evolve the mean curvature equation for this function, producing a minimal surface as the final limiting state. We use this technique to study the minimal surface spanning two parallel rings close to one another, and compare the result to the known exact solution, the catenoid. We then pull the rings apart and repeat the experiment; in this case the surface must pinch and break (change topology), the final configuration being two disks. We consider other wire frames as well.

In Section 5 we compute surfaces of constant nonzero mean curvature by adding a hyperbolic component to the partial differential equation describing the flow. As examples, we compute catenoid-like surfaces of a variety of nonzero curvatures. We also extend the level set formulation to the computation of surfaces of any prescribed function of the curvature.

Finally, Section 6 generalizes the curvature flow algorithm to curves on surfaces in $\mathbb{R}^3$, the speed being made to depend on the geodesic curvature of the curve. We test the flow for curves on a cube, a sphere, and a torus. The techniques used for computing minimal surfaces can be adapted to this setting, creating an algorithm for computing the geodesics of a manifold.

In summary, this paper extends and applies the level set approach to complex surfaces, flows under Gaussian curvature, computation of surfaces of nonconstant curvature, and geodesics on manifolds. We hope that some of the complex and subtle phenomena exposed in this paper may lead to further conjectures and better understanding of curvature-driven flow.

This article first appeared as a technical report of the Center for Pure and Applied Mathematics at Berkeley. Examples from that work contributed to an overview report that appeared in the Computational Crystal Growers Workshop [Sethian and Chopp 1992].

2. THE LEVEL SET FORMULATION

2.1. Equations of Motion

To begin with, we consider a one-parameter family of closed curves γ in $\mathbb{R}^2$, where the parameter $t \in [0, \infty)$ is thought of as time. We assume the motion of each point of the curve to be normal to the curve. Its speed F may depend on local properties such as the curvature or normal vector, depending on the problem being modeled; typically the curve represents the interface between two phases. The goal is to describe $\gamma(t)$, given the initial curve $\gamma(0)$ of the family.

The *level set formulation* of this problem [Osher and Sethian 1988] is illustrated in Figure 1, for $\gamma(t)$ a circle in the xy-plane propagating outwards with constant speed. We express $\gamma(0)$ as the zero set of a function of x and y, here $r_0 - \sqrt{x^2 + y^2}$, where r_0 is the radius of the initial circle. Then we let this function evolve with t in the appropriate way, obtaining a function $\varphi(x, y, t)$ such that $\gamma(t)$, for each t, is still the level set of $\varphi(x, y, t)$ (considered as a function of x and y).

The origins of this approach lie in [Sethian 1985; Sethian 1987], where the role of curvature in the speed function F was shown to be analogous to the

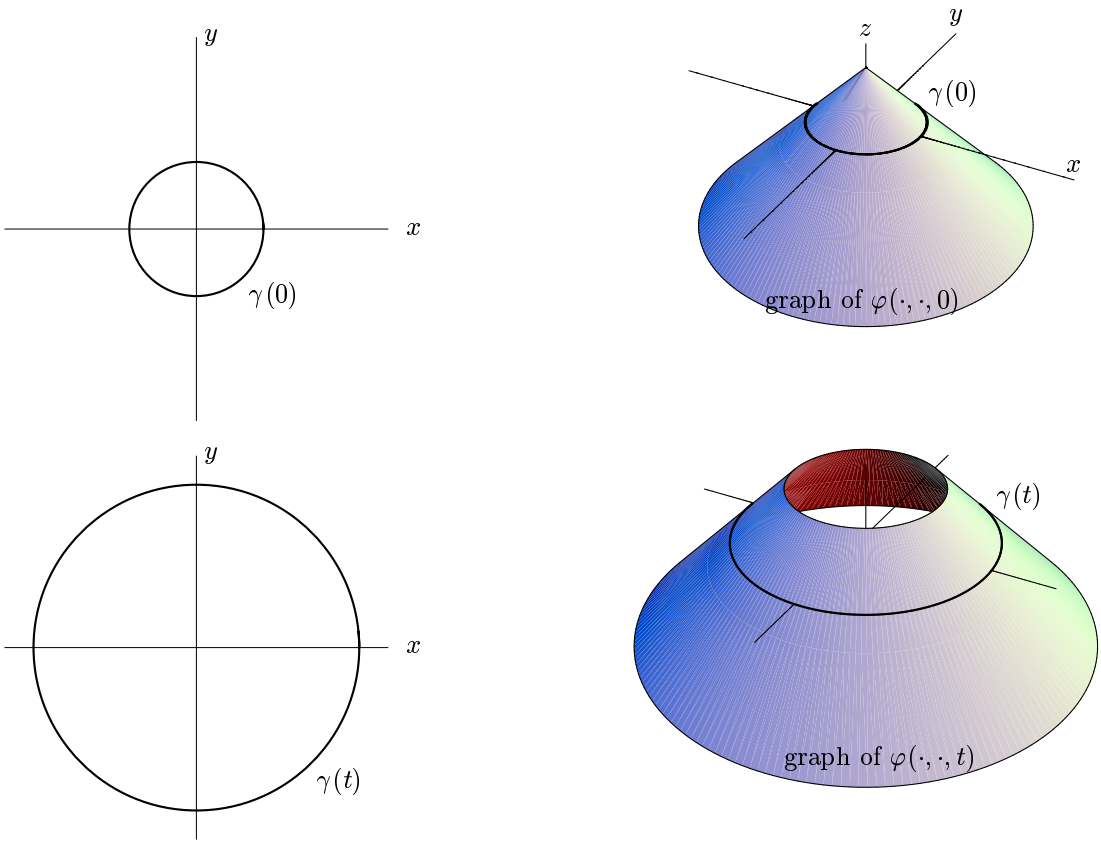

FIGURE 1. The evolution of the curve $\gamma(t)$ (left) is described in terms of a function φ of which γ is the zero set (right). Here $\gamma(t)$ is a circle of radius $t + r_0$, and $\varphi(x, y, t) = t + r_0 - \sqrt{x^2 + y^2}$.

role of viscosity in the corresponding hyperbolic conservation law for the evolving slope of the curve.

In general terms, let $\gamma(0)$ be a closed, nonintersecting, $(N-1)$-dimensional hypersurface in $\mathbb{R}^n$, and construct a function $\varphi(\bar{x}, t)$ from $\mathbb{R}^N$ to $\mathbb{R}$ such that the level set $\{\varphi = 0\}$ is the front $\gamma(t)$:

$$\gamma(t) = \{\bar{x} \in \mathbb{R}^N : \varphi(\bar{x}, t) = 0\}.$$

To construct such a function $\varphi(\bar{x}, t)$, we must have appropriate initial conditions $\varphi(\bar{x}, 0)$ and an associated partial differential equation for the time evolution of $\varphi(\bar{x}, t)$. We can initialize φ by

$$\varphi(\bar{x}, 0) = \pm d(\bar{x}), \tag{2.1}$$

where $d(\bar{x})$ is the signed distance from $\bar{x}$ to the initial front $\gamma(0)$. In order to derive the partial differential equation for the time evolution of φ, consider the motion of a level set $\{\varphi(\bar{x}, t) = C\}$. Let $\bar{x}(t)$ be the trajectory of some particle located on this level set, so that

$$\varphi(\bar{x}(t), t) = C$$

[Mulder et al. 1992]. The particle velocity $\partial\bar{x}/\partial t$ in the direction normal to the level set C is

$$\frac{\partial \bar{x}}{\partial t} \cdot \bar{n} = F,$$

where $\bar{n} = \nabla\varphi / \|\nabla\varphi\|$ is the normal vector. By the chain rule,

$$\varphi_t + \frac{\partial \bar{x}}{\partial t} \cdot \nabla\varphi = 0,$$

and substitution yields

$$\varphi_t + F \, \|\nabla\varphi\| = 0. \tag{2.2}$$

Thus, (2.2) describes the motion of the interface $\gamma(t)$ as the level set $\varphi = 0$. We call this the *level set formulation.*

For certain speed functions, (2.2) reduces to familiar equations. For $F = 1$, it becomes the eikonal equation for a front moving with constant speed. For $F = 1 - \varepsilon\kappa$, where κ is the curvature of the front, (2.2) becomes a Hamilton–Jacobi equation with parabolic right-hand side, similar to those discussed in [Crandall and Lions 1983]. For $F = \kappa$, (2.2) reduces to the equation for mean curvature flow.

When required, the curvature κ may be determined from the level set function φ. For example, in $\mathbb{R}^3$ the mean curvature is

$$\begin{aligned}\kappa = {} & \tfrac{1}{2}(\varphi_x^2 + \varphi_y^2 + \varphi_z^2)^{-3/2} \\ & \times \big(\varphi_{xx}(\varphi_y^2 + \varphi_z^2) + \varphi_{yy}(\varphi_x^2 + \varphi_z^2) + \varphi_{zz}(\varphi_x^2 + \varphi_y^2) \\ & \quad - 2(\varphi_x\varphi_y\varphi_{xy} + \varphi_y\varphi_z\varphi_{yz} + \varphi_x\varphi_z\varphi_{xz})\big).\end{aligned} \tag{2.3}$$

Equation (2.2) is an Eulerian formulation for the hypersurface propagation problem, because it is written in terms of a fixed coordinate system in the physical domain. This is in contrast to a more geometry-based Lagrangian approach, in which the motion of the hypersurface is written in terms of a parametrization in $(N-1)$-dimensional space. There are several advantages to the Eulerian approach given in (2.2): the fixed coordinate system avoids the numerical stability problems that plague approximation techniques based on a parametrized approach; topological changes are handled naturally, since the level surface $\varphi = 0$ need not be simply connected; finally, the formulation clearly applies in any number of space dimensions.

This level set approach to front propagation has been employed in a variety of investigations. In numerical settings, it has been used to study flame propagation [Zhu and Sethian 1992] and crystal growth and dendrite simulation [Sethian and Strain 1992]. The theoretical underpinnings of this approach have been examined in detail in [Evans and Spruck 1991; 1992]; for further theoretical work, see also [Chen et al. 1991; Evans et al. 1992; Falcone et al. 1990; Giga and Goto 1992].

2.2. Numerical Approximation

A successful numerical scheme to handle (2.2) will hinge on the already mentioned link with hyperbolic conservation laws. As motivation, consider the simple case of a moving front in two space dimensions that remains a graph as it evolves, the initial front being the graph of a function $f(x)$ periodic of period 1. Let $y(x,t)$ be the height of the propagating function at time t, so that $y(x,0) = f(x)$. The normal at (x,y) is $(-y_x, 1)$, and the equation of motion becomes $y_t = F(\kappa)\sqrt{1+y_x^2}$. Using the speed function $F(\kappa) = 1 - \varepsilon\kappa$, where the curvature κ equals $y_{xx}(1+y_x^2)^{-3/2}$, we get

$$y_t - \sqrt{1+y_x^2} = \varepsilon\frac{y_{xx}}{(1+y_x^2)}.$$

To construct an evolution equation for the slope $u = dy/dx$, we differentiate both sides with respect to x and substitute to obtain

$$\frac{\partial u}{\partial t} - \frac{\partial}{\partial x}\sqrt{1+u^2} = \varepsilon\frac{\partial}{\partial x}\Big(\frac{\partial u/\partial x}{1+u^2}\Big).$$

Thus, the derivative of the Hamilton–Jacobi equation with curvature-dependent right-hand side for the changing height $y(x,t)$ is a viscous hyperbolic conservation law for the propagating slope u. With this hyperbolic conservation law, an associated entropy condition must be invoked to produce the correct weak solution beyond the development of a singularity in the evolving curvature. For details, see [Sethian 1989].

Consequently, considerable care must be taken in devising numerical schemes to approximate the level set (2.2). Because a central difference approximation to the gradient produces the wrong weak solution, we instead exploit the technology of hyperbolic conservation laws in devising schemes that maintain sharp corners in the evolving hypersurface and choose the correct, entropy-satisfying weak solution.

FIGURE 2. Spiral collapsing under $F(\kappa) = -\kappa$. The initial curve is $(e^{-y(s)} + .05\cos 2\pi s)(\cos a(s), \sin a(s))$, where $a(s) = 25 \arctan y(s)$ and $y(s) = .5 \sin 2\pi s + 1$. The grid is 200×200.

One of the easiest such schemes is a variation of the Engquist–Osher scheme presented in [Osher and Sethian 1988]. This scheme is upwind in order to follow the characteristics at boundaries of the computational domain. It goes as follows. Decompose the speed function F into $F = F_A + F_B$, where F_A is treated as the hyperbolic component that must be handled through upwind differencing, and F_B is a remainder that is to be approximated through central differencing. Let φ^n_{ijk} be the numerical approximation to the solution φ at the point $(i\Delta x, j\Delta y, k\Delta z)$ and at time $n\Delta t$, where Δx, Δy, Δz is the grid spacing and Δt is the time step. We can then advance from one time step to the next as follows: to go from φ^n_{ijk} to φ^{n+1}_{ijk}, add

$$\begin{aligned} F_A \Delta t \; \big(&\min(D_x^- \varphi_{ijk}, 0)^2 + \max(D_x^+ \varphi_{ijk}, 0)^2 \\ &+ \min(D_y^- \varphi_{ijk}, 0)^2 + \max(D_y^+ \varphi_{ijk}, 0)^2 \\ &+ \min(D_z^- \varphi_{ijk}, 0)^2 + \max(D_z^+ \varphi_{ijk}, 0)^2 \big)^{1/2} \\ + \Delta t \, F_B \|\nabla \varphi\|. \end{aligned} \tag{2.4}$$

Here D_x^- refers to the backward difference in the x-direction, and the other difference operators are defined similarly.

2.3. Examples

Figure 2 shows the motion of a closed spiral in two dimensions collapsing under its own curvature: $F(\kappa) = -\kappa$. Grayson [1987] has shown that any nonintersecting closed curve must collapse smoothly to a circle; see also [Gage 1983; 1984; Gage and Hamilton 1986].

Note that the calculation follows a family of spirals lying on the higher-dimensional surface. The particular front corresponding to the propagating curve vanishes when the graph of φ moves entirely above the xy-plane, that is, when $\varphi^n_{ij} > 0$. This illustrates the point about changes in the topology of the front being handled naturally.

Now if we let the same spiral evolve with speed $F(\kappa) = 1 - \varepsilon\kappa$, with $\varepsilon = 0.1$, the evolution is quite different, as shown in Figure 3. Here the entropy condition is needed in order to account for the change in topology as the front burns together.

FIGURE 3. Spiral "flame" spreading under $F(\kappa) = 1 - .1\kappa$. The initial curve (not shown) and the grid are the same as in Figure 2. As the spiral expands, it separates into two flames (boundary components), one propagating outwards and one inwards. The inner front collapses and disappears, and all that remains is the outer front, which asymptotically approaches a circle.

3. SINGULARITY FORMATION IN CURVATURE FLOW

3.1. Collapsing Dumbbells under Mean Curvature Flow

This section studies singularity formation of surfaces in three-space propagating under mean curvature. Such flows were treated theoretically in [Brakke 1992; Grayson 1989; Huisken 1984], while [Brakke 1978] includes numerical calculations based on a marker Lagrangian approach.

A well-known example is the collapse of a dumbbell [Sethian 1989]. Figure 4 shows the evolution of the cross-section of a dumbbell collapsing under its mean curvature ($F(\kappa) = -\kappa$).

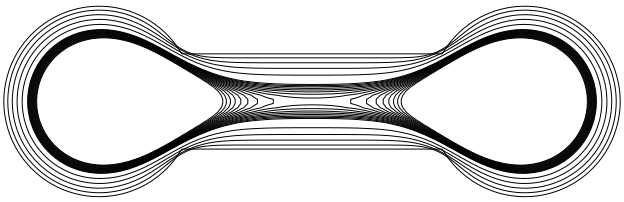

FIGURE 4. Cross-section of rotationally symmetric dumbbell, collapsing under the action of mean curvature. The handle pinches off, separating the surface into two pieces, which continue to shrink and eventually vanish. The grid is $214 \times 72 \times 72$.

An extension of this problem can be seen in Figure 5, where a periodic link of dumbbells is considered. As can be seen from the figures, each handle pinches off and breaks, leaving a collection of separate periodic closed surfaces that each collapse into a sphere.

A different picture emerges if we consider many-armed dumbbells. The left column of Figure 6 shows a three-armed dumbbell. As this surface collapses under its mean curvature, the three handles pinch off, leaving a separate closed surface in the center. This "pillow" occurs because the mean curvature of each handle is larger than the saddle joints in the webbing between the spikes. Once this pillow separates off, it quickly collapses to a point.

More pronounced versions, involving dumbbells with four and six arms, are shown in the other two columns of Figure 6. Once again, a residual pillow separates off in the center and collapses smoothly

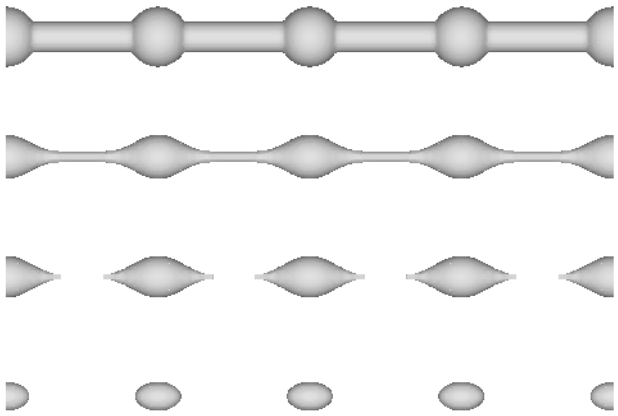

FIGURE 5. Collapse of a dumbbell string under mean curvature. The snapshots are taken at $t = 0$, 0.35, 0.355 and 0.655.

through a spherical shape to a point. The separated pillow is larger because the webbing between the arms collapses slower as the number of arms increases. For the six-armed dumbbell, the pillow is almost the same size as the collapsing end balls.

To verify that the appearance of the central pillow is not a numerical artifact, we compared its behavior as the grid was refined. The following table lists the diagonal span and the volume of the pillow as soon as it detaches itself. It is apparent that the shape and dimensions are essentially independent of the grid size, and so should be preserved under passage to the limit.

grid size	diagonal	volume
$30 \times 30 \times 10$	.35012	.00863
$46 \times 46 \times 16$	.34105	.00964
$61 \times 61 \times 60$	.35181	.01058
$61 \times 61 \times 61$	.35214	.01063

As a final demonstration of this process, Figures 7 and 8 show the collapse of lattices of tubes. The experiment was run with periodic boundary conditions, so each figure represents one section of an infinite lattice. When the tubes have small diameter (Figure 7), they collapse, while pillows emerge at their intersections. The pillows then

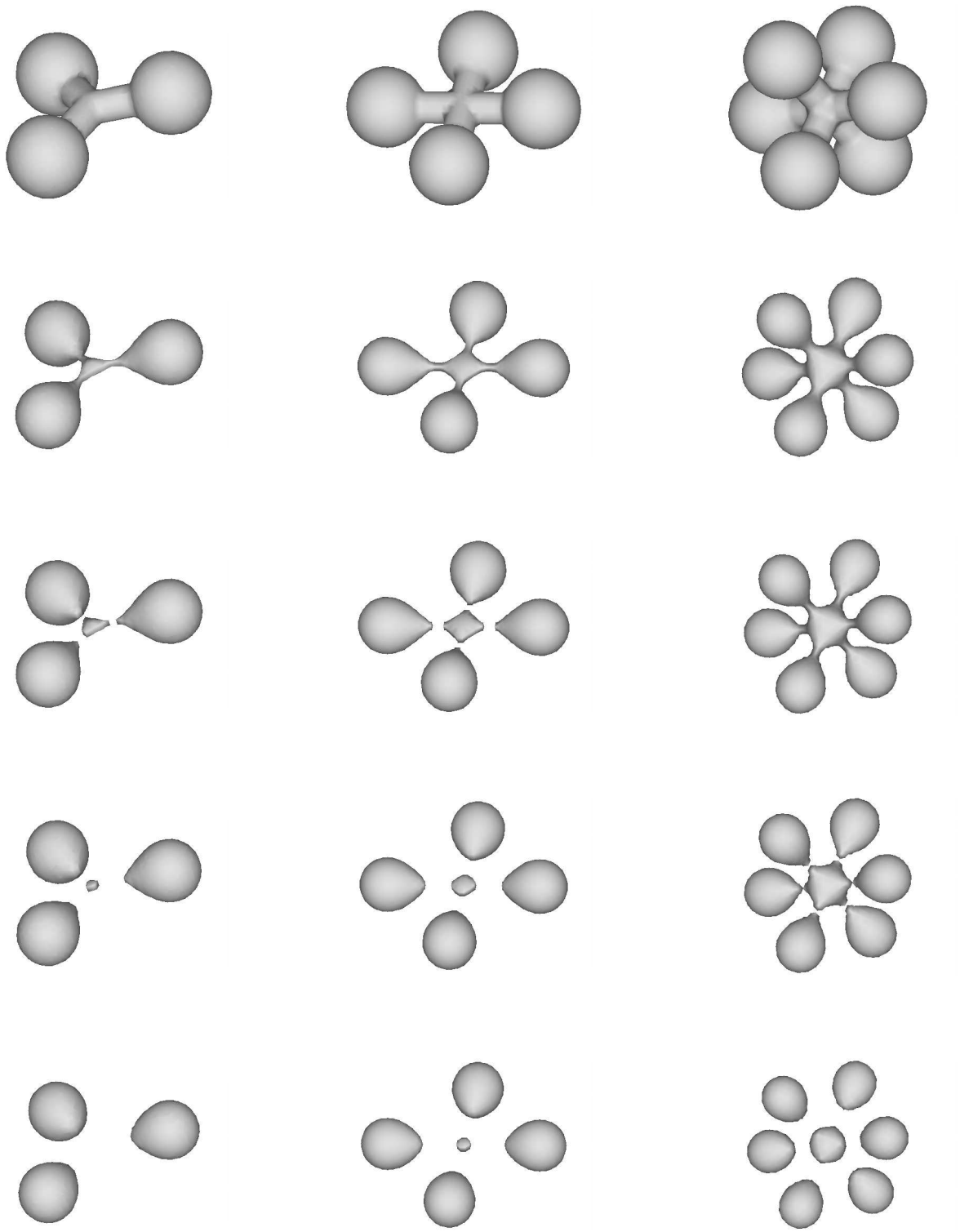

FIGURE 6. Collapse of many-armed dumbbells under mean curvature.

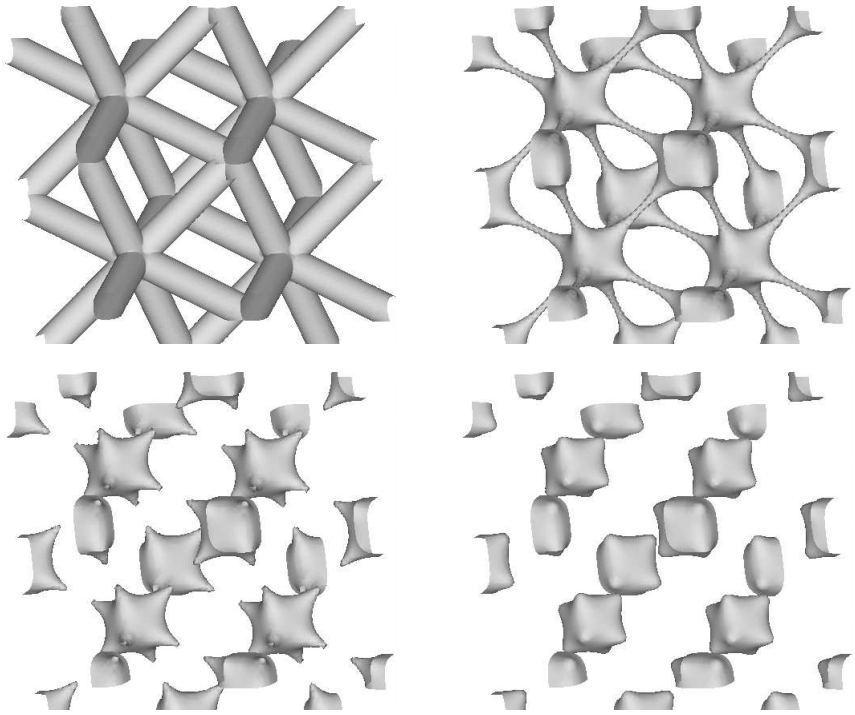

FIGURE 7. Evolution of a lattice of thin tubes, showing the emergence of pillows at the intersections, while the tubes pinch off. The snapshots are taken at $t = 0$, 0.385, 0.405 and 0.455.

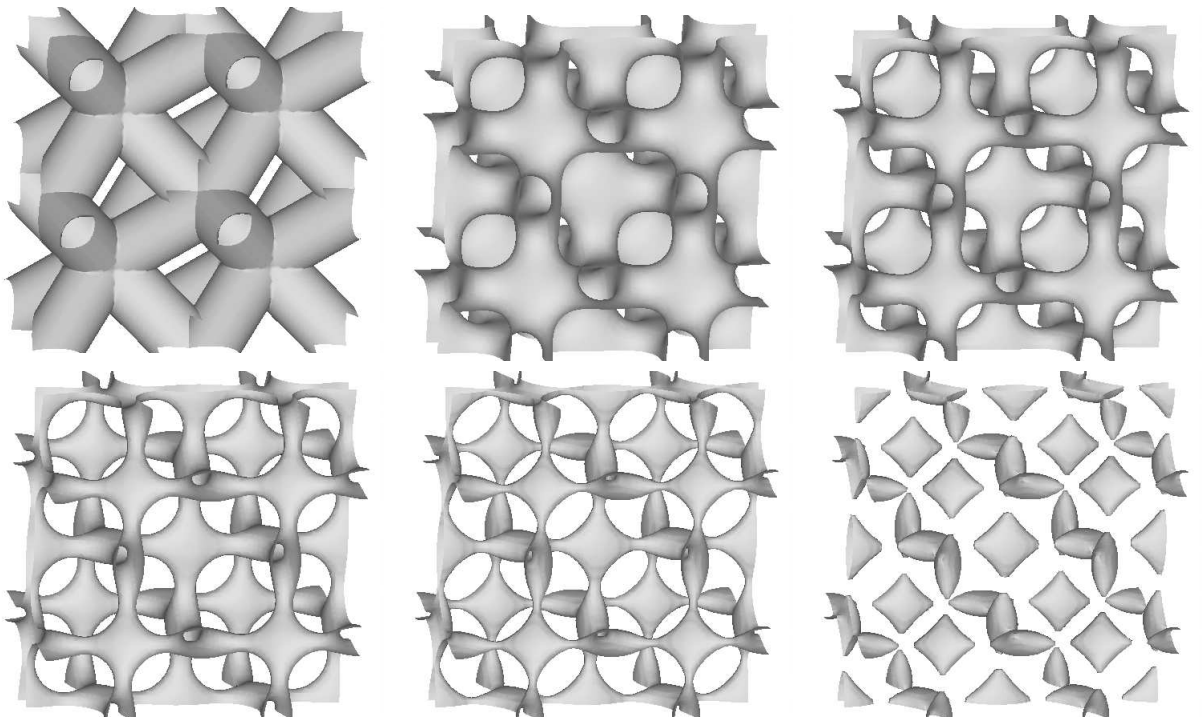

FIGURE 8. Evolution of a lattice of thick tubes, showing the emergence of pillows complementary to those of Figure 7.

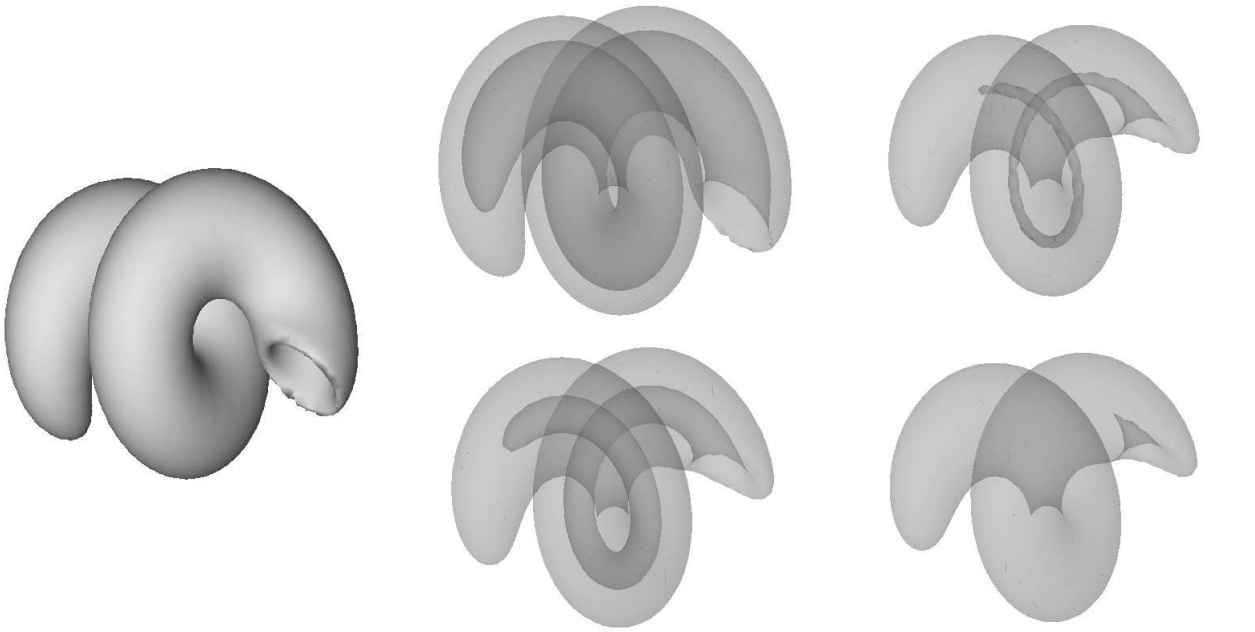

FIGURE 9. Collapse of a twisted test tube. On the left, the initial surface is shown opaque; on the right, the evolution is shown using transparency (darker shades indicate more sheets across the line of sight). The inner wall of the tube shrinks faster than the outer one, and withdraws to the rightmost edge, leading to the shape on the lower right. This shape will continue to collapse while becoming more spherical.

quickly evolve towards spherical shapes and finally collapse too. In contrast, when the tubes are thick (Figure 8), pillows appear in the *holes* of the lattice, as the evolving surface collapses around them.

Finally, Figure 9 shows a three-dimensional version of the spiral of Figure 2, collapsing under mean curvature. The initial surface is homeomorphic to a sphere: the region it bounds looks like a twisted test tube, the opening on the right extending almost all the way through the object. The inner and outer walls of the tube are separated by only a short distance.

3.2. Collapsing Surfaces under Gaussian Curvature Flow

As a variation on the above study, we can use the Gaussian curvature instead of the mean curvature to control the flow. The expression of the Gaussian curvature in terms of the level set function φ is

$$\frac{2\varphi_x\varphi_y(\varphi_{xz}\varphi_{yz} - \varphi_{xy}\varphi_{zz}) + \varphi_{xx}(\varphi_y^2 + \varphi_z^2) + \cdots}{(\varphi_x^2 + \varphi_y^2 + \varphi_z^2)^2},$$

the ellipses representing four terms obtained from the two preceding ones by cyclic permutation of the indices.

For a closed, convex surface flowing under this type of flow, the sign of the Gaussian curvature will not change, and the surface should collapse. This is illustrated in Figure 10; see also [Oliker 1991]. The sharply curved regions move in quickly, since they are regions of high Gaussian curvature, and the surface moves towards a spheroidal shape.

For nonconvex closed surfaces, the situation is more complicated, because the Gaussian curvature is the product of the two principle curvatures. In general, the problem acts like the backwards heat equation, and goes unstable in most cases. We illustrate with two examples. In Figure 11, a very slightly depressed dumbbell is shown. The balls have radius .5, while the inner handle has radius .45. The distance between the centers of the two end balls is 2. Because the variation away from a cylindrical shape is small, the strong positive Gaussian curvature on the ends pulls the surface

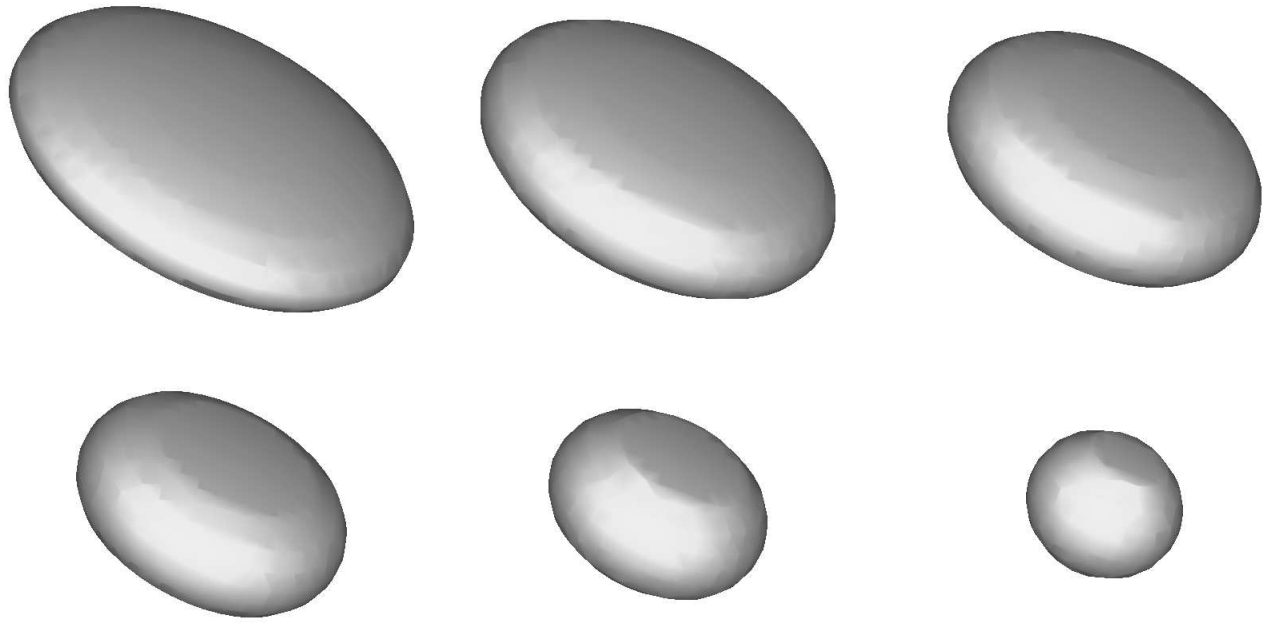

FIGURE 10. Evolution of a convex surface under Gaussian curvature.

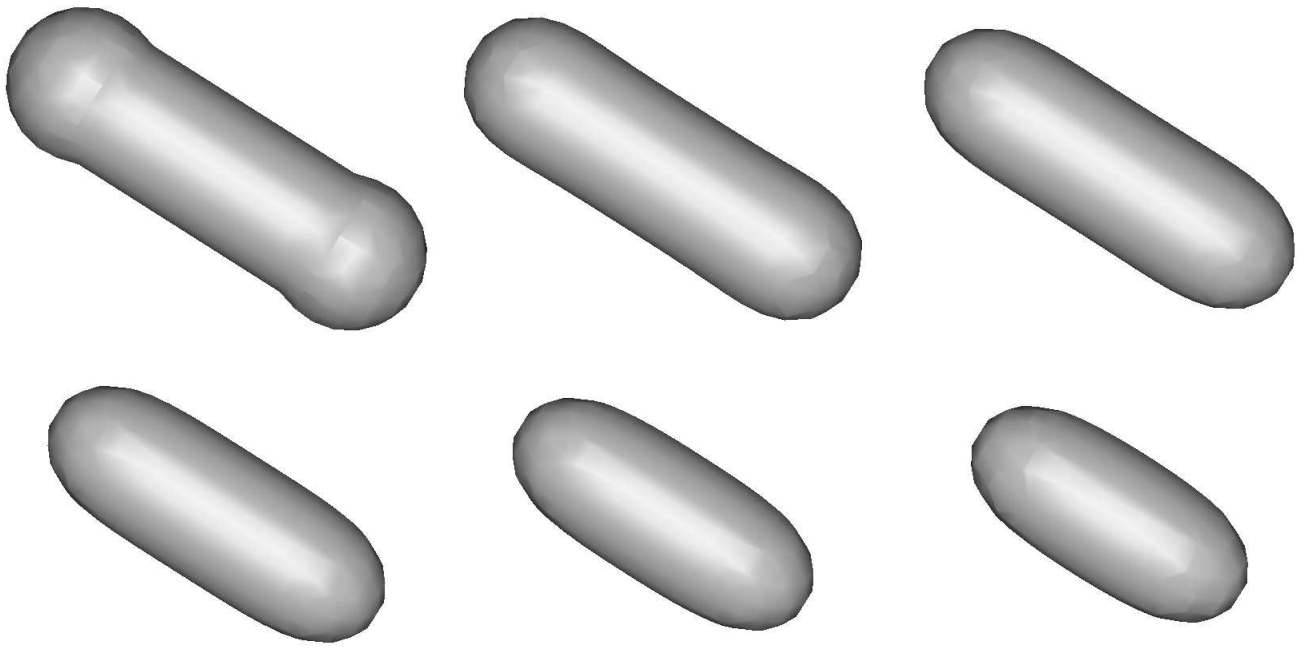

FIGURE 11. Evolution of a slightly nonconvex surface under Gaussian curvature.

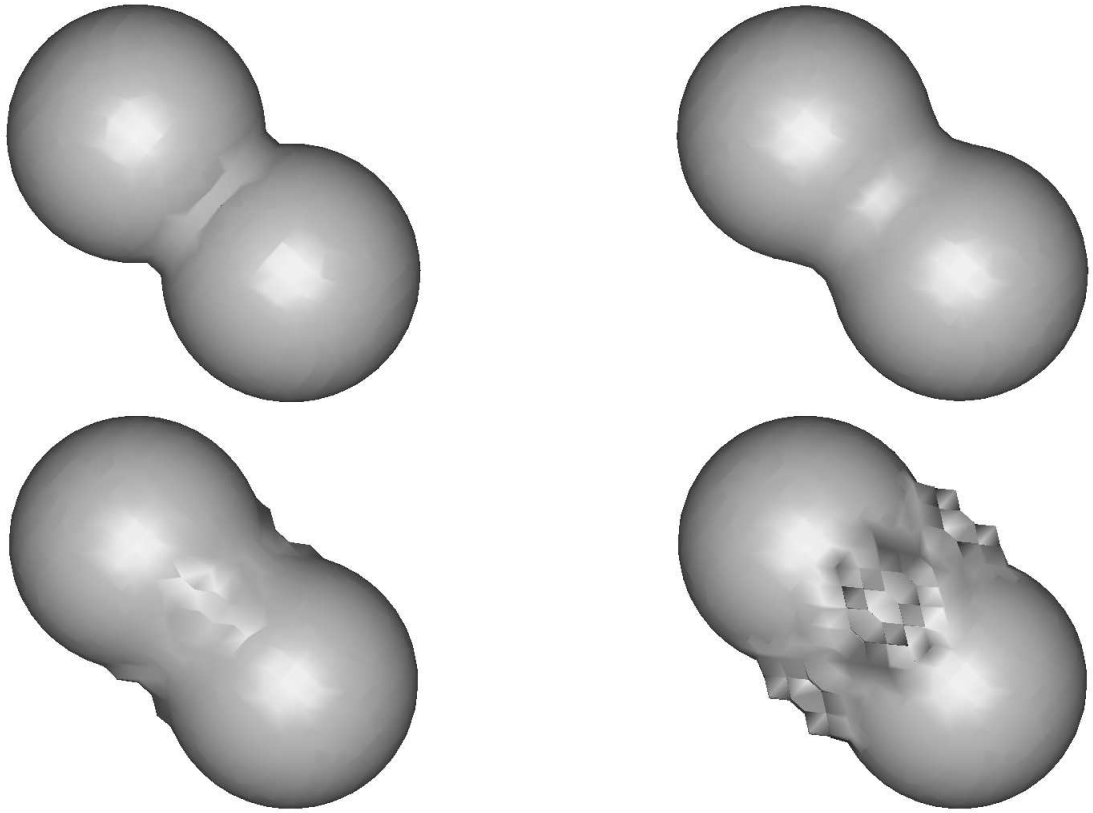

FIGURE 12. Evolution of a more nonconvex surface under Gaussian curvature.

inwards, and it seems that the calculation remains stable and the surface collapses. In contrast, Figure 12 shows the evolution of two spheres glued together by means of a narrow connecting ring. The Gaussian curvature along the edges of the ring is initially large and negative. This carries the indentation area outwards, and instability develops.

4. CONSTRUCTION OF MINIMAL SURFACES

In this section we use the level set formulation to construct minimal surfaces. Consider a closed curve $\Gamma : [0,1] \to \mathbb{R}^3$. The goal is to construct a membrane with boundary Γ and mean curvature zero.

Let $S(0)$ be some initial surface whose boundary is Γ. Let $S(t)$ be the family of surfaces obtained by allowing $S(0)$ to evolve under mean curvature, subject to the constraint that the boundary remains Γ for all time t. Assuming this family has a limit S as $t \to \infty$, we can expect S to be a minimal surface for the boundary Γ.

Thus, given an initial surface $S(0)$ going through Γ, we construct a family of neighboring surfaces by viewing $S(0)$ as the zero level set of some function φ over all of $\mathbb{R}^3$. Using the level set equation (2.2), we evolve φ according to the speed law $F(\kappa) = -\kappa$. Then the minimal surface S will be given by

$$S = \lim_{t\to\infty} \{\bar{x} : \varphi(\bar{x}, t) = 0\}$$

The challenge with this approach is to ensure that the evolving zero level set always remains attached to the boundary Γ. This is accomplished by creating a set of boundary conditions on those grid points closest to the wire frame, and linking together the neighboring values of φ to force the level set $\varphi = 0$ to go through Γ. The underlying idea is most easily explained through a one-dimensional example. We follow the discussion in [Chopp 1993].

Consider the simple problem of finding a curve of minimal length between two points A and B in the plane, using the level set approach. We must ensure that the function $\varphi : \mathbb{R}^2 \to \mathbb{R}$ satisfies $\varphi(A,t) = \varphi(B,t) = 0$ for all t. However, we only have control over φ at the points of the chosen mesh. To ensure, for example, that $\varphi(A,t) = 0$, we express $\varphi(A,t)$ as a linear combination of values of φ at adjacent mesh points, and enforce the condition that this combination must vanish. Thus, if A lies exactly halfway between two neighboring mesh points g and g', we require that $\varphi(g,t) = -\varphi(g',t)$ for all t. One of g, g' is chosen to be an independent point; the other is a dependent point, that is, the value of φ there is determined by the value of φ at the other mesh point.

In general, the boundary conditions will be represented as an equation of the form

$$\begin{pmatrix} \varphi(g_{d,1}) \\ \varphi(g_{d,2}) \\ \vdots \\ \varphi(g_{d,m}) \end{pmatrix} = A \begin{pmatrix} \varphi(g_{i,1}) \\ \varphi(g_{i,2}) \\ \vdots \\ \varphi(g_{i,n}) \end{pmatrix},$$

where the $g_{d,k}$ are the mesh points declared dependent, the $g_{i,k}$ are the mesh points declared independent, and A is an appropriate $m \times n$ matrix. A is determined from the chosen mesh and wire frame, and hence its determination, and the choice of dependent and independent mesh points, need only be made once, at the beginning of the calculation. This links the set of all dependent points in terms of the set of all independent points, in such a way that the level set $\varphi = 0$ is forced to pass through the wire frame. Details of the automatic technique for generating this list of boundary conditions may be found in [Chopp 1993].

There is one final issue that comes into play in the evolution of the level set function φ towards a minimal surface. The above set of boundary conditions only constrains the zero set of φ. Thus the other level sets are free to move at will, which means that they may crowd together on one side of the zero set, while on the other side they may pull away. This causes numerical difficulties in the evaluation of derivatives over such a steep gradient. A reinitialization procedure is used to remedy this; after a given number of time steps, the zero set is computed, and the function φ is reinitialized using the signed distance function (2.1).

As a test example, we compute the minimal surface spanning two equal rings parallel to the yz-plane and centered at two points of the x-axis symmetric about the origin. The exact solution to this problem, if it exists, is a piece of the catenoid

$$r(x) = a \cosh(x/a),$$

where $r(x)$ is the radius of the section parallel to the yz-plane and at distance x from the origin, and a is the radius of the section by the yz-plane. Suppose the rings have radius R and are located at $\pm b$ on the x-axis. Then a satisfies $R = a\cosh(b/a)$. Now, for R fixed, $b = a\,\mathrm{arccosh}(R/a)$ is a concave function of a that vanishes at $a = 0$ and $a = 1$; let its maximum be $b_{\max}$. If the distance between the rings is less than $2b_{\max}$, there are two solutions for a and thus two catenoid solutions, one stable and one unstable. For rings exactly $2b_{\max}$ apart, there is only one solution. For rings more than $2b_{\max}$ apart, there is no catenoid solution.

Figure 13 shows various views of the solution with $R = 0.5$ and $b = .277259$, obtained from a cylindrical initial surface. Figure 14 shows the evolution of the same initial surface when the rings are far apart: the middle pinches off and the surface splits into two, each of which quickly collapses to a disk. (A disk spanning each ring is indeed a minimal surface for this problem.)

Figure 15 shows the breakup of a surface that spans six squares, each pair being separated by a different distance. More complex examples of minimal surfaces are given in [Chopp 1993].

These examples illustrate one of the virtues of the level set approach. No special cutting or *ad hoc* decisions are employed to decide when to break the surface. Instead, the characterization of the zero

FIGURE 13. Catenoid spanning rings of radius .5 and separated by the distance $2 \times .277259$. The initial approximation was a cylinder. The mesh used had step 0.025 along each coordinate, and its size was $27 \times 47 \times 47$.

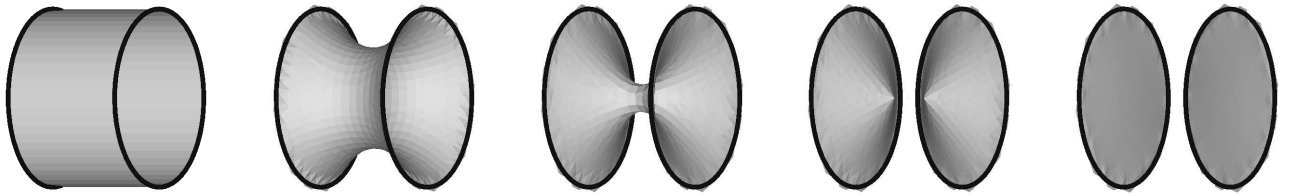

FIGURE 14. When the rings are further apart, a catenoid solution does not exist; instead the initial cylinder pinches in the middle and splits. Times shown are $t = 0$, 0.2, 0.41, 0.42 and 0.50.

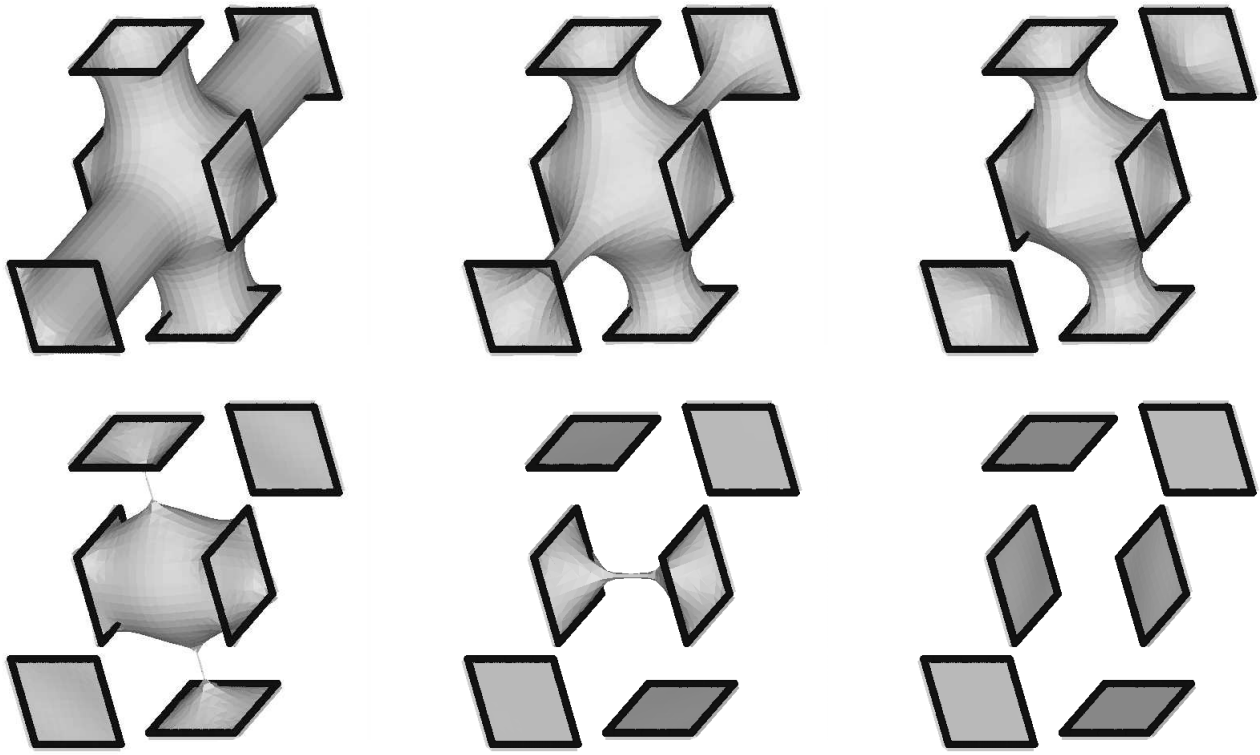

FIGURE 15. Evolution of surface spanning six squares; the initial stage (not shown) is the union of three cylinders with square cross-sections. Each square has side length .5. On the x-axis, the squares are located at ± 0.375, on the y-axis at ± 0.775, and on the z-axis at ± 1.275. The different distances cause the surface to break at three different times. The snapshots are taken at times $t = 0.01$, 0.03, 0.04, 0.06, 0.10 and 0.13.

level set as but one member of a family of flowing surfaces allows this smooth transition.

5. EXTENSIONS TO SURFACES OF PRESCRIBED CURVATURE

5.1. Surfaces of Constant Mean Curvature

The above technique can be extended to produce surfaces of constant but nonzero mean curvature. To do so requires further inspection of the suggestive example of a front propagating with speed $F(\kappa) = 1 - \varepsilon\kappa$. Suppose that $\varepsilon = 1$, and consider the evolution of the partial differential equation

$$\varphi_t = (1 - \kappa)\|\nabla\varphi\|,$$

where again the mean curvature κ is given by (2.3). Furthermore, consider initial data given by

$$\varphi(x, y, z, 0) = (x^2 + y^2 + z^2)^{1/2} - 1$$

The zero set is the sphere of radius one, which remains fixed under the motion $F(\kappa) = 1 - \kappa$. All level surfaces inside the unit sphere have mean curvature greater than one, and hence propagate inwards, while all level surfaces outside the unit sphere have mean curvature less than one, and hence propagate outwards. Thus, the level sets on either side of the zero set pull apart.

If one were to apply the level set algorithm in free space, the gradient $\|\nabla\varphi\|$ would smooth out to zero along the unit sphere surface, and this eventually causes numerical difficulties. However, the reinitialization process described earlier can be used to periodically relabel level sets, thus renormalizing $\|\nabla\varphi\|$.

Thus, in order to construct a surface of constant curvature κ_0, we start with any initial surface passing through the initial wire frame and allow it to propagate with speed

$$F(\kappa) = \kappa_0 - \kappa.$$

Here, as before, the "constant advection term" κ_0 is taken as the hyperbolic component F_A in 2.4, and treated using the entropy-satisfying upwind difference solver, while the parabolic term κ is assigned to F_B, and is approximated using central differences.

Figure 16 shows the results of applying this technique to the "catenoid" problem. For two fixed boundary rings, various values of the mean curvature κ_0 are prescribed; there is a stable connected surface of that curvature spanning both rings if κ_0 is not too negative or too positive. Note that the signs of the principal curvatures (of which the mean curvature is the average) take into account the orientation of the surface; thus a pair of spherical caps spanning the rings, bulging in if $\kappa_0 > 0$ and out if $\kappa_0 < 0$, form a solution. When κ_0 is very negative and there is no connected solution, the system tends toward this configuration, as shown by the last two images in Figure 16.

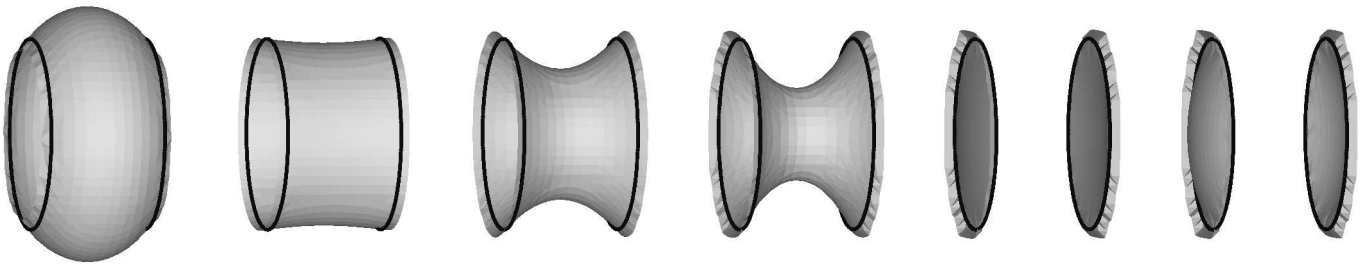

FIGURE 16. Surfaces of constant mean curvature κ_0 with fixed boundary, obtained by evolution of a cylindrical initial surface under the action of $F(\kappa) = \kappa_0 - \kappa$. The rings have diameter 1 and the distance between them is .61. The exact solution for $\kappa_0 = 1$ is the initial cylinder itself; the slight bowing is due to the relatively coarse $40 \times 40 \times 40$ mesh. Note the abrupt change in regime somewhere around $\kappa_0 = -0.34$.

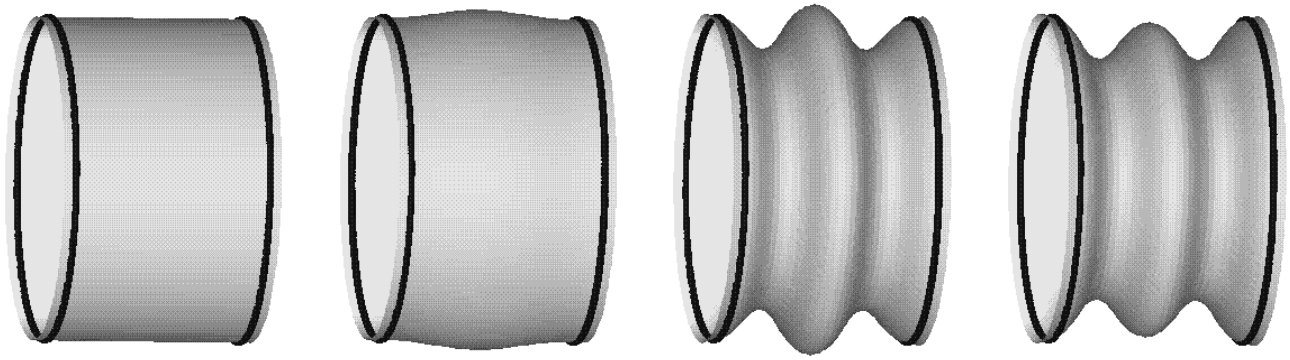

FIGURE 17. Surface of nonconstant prescribed curvature, $\kappa_0 = 10\cos 10x$. The grid size is $40 \times 75 \times 75$, with step 0.02. The rings are located at ± 0.305, with radius .5. After 100 time steps, the change in φ is less than 10^{-5} per time step of size 10^{-4}, indicating convergence.

5.2. Surfaces of Non-Constant Mean Curvature

We now extend the technique to allow the calculation of surfaces with curvature a function of position. Suppose we wish to find a surface passing through a given wire frame and having mean curvature $\kappa_0(\bar{x})$, where κ_0 is now a prescribed function $\mathbb{R}^3 \to \mathbb{R}$. Using the above approach, we simply evolve the initial zero surface with speed

$$F(\kappa) = \kappa_0(\bar{x}) - \kappa.$$

As an example, we construct the surface spanning two rings and having curvature depending on the x-coordinate: $\kappa_0 = 10\cos 10x$. Figure 17 shows the wavy surface obtained.

6. GEODESIC CURVATURE FLOW

The curvature flow algorithm can be generalized to more complicated two-dimensional spaces. For example, we may let the level set function φ be defined on a differentiable two-manifold in $\mathbb{R}^3$ with speed depending on geodesic curvature. By restricting φ to coordinate patches, one can study single curves on non-simply connected manifolds such as a torus. The fixed boundary condition techniques for minimal surfaces can also be applied here. In this case, a curve with fixed endpoints should flow towards a curve of zero geodesic curvature, that is, a geodesic of the manifold.

6.1. Equations of Motion

Consider a two-dimensional manifold $M \subset \mathbb{R}^3$. Let $\gamma(t) \subset M$, for $t \in [0, \infty)$, be a family of closed curves moving with speed $F(\kappa_g)$ in the direction normal to itself on M. Here, κ_g is the geodesic curvature of $\gamma(t)$ on M. Let $g_t(s)$ be the parametrization of $\gamma(t)$ by arc length.

First assume that M is orientable. In this case, the unit normal map N is continuous on M. At every point $g_t(s)$, a natural coordinate system for T_M is given by the pair of vectors $(g_t'(s),\ N \times g_t'(s))$. Thus, for any point $x(t) \in \gamma(t)$, the velocity under this flow is

$$\dot{x} \cdot (N \times g_t') = F(\kappa_g).$$

The expression for the geodesic curvature is

$$\kappa_g = (N \times g_t') \cdot g_t''.$$

Note that a change in sign of the unit normal N results in a corresponding change in sign of κ_g. If F is an odd function, $\dot{x}$ is independent of the choice of N. Otherwise, the choice of the normal changes the flow. Therefore, if M is not orientable, only odd speed functions F are allowed. The algorithm presented here also requires that F be an odd function when M is not simply connected.

Assume that $M = f^{-1}(0)$, where $f : \mathbb{R}^3 \to \mathbb{R}$. We break the manifold into a collection of coordinate maps $\{(U_i, \pi_i)\}$ such that $M = \bigcup U_i$, each

set U_i is simply connected, and $\pi_i : U_i \to V_i \subset \mathbb{R}^2$ is a homeomorphism. The computing is done on the collection of sets $V_i = \pi_i(U_i)$. We define the function $\Phi_i : V_i \to \mathbb{R}$ by $\Phi_i(x,t) = \varphi(\pi_i^{-1}(x),t)$, so that $\varphi(x,t)|_{U_i} = \Phi_i(\pi_i(x),t)$.

In order to write the equations of motion in the level set representation, we must compute a velocity field on the entire manifold M. We compute the velocity field on each coordinate patch and then check that it is consistent in regions of overlap. For this section, assume $\varphi = \varphi|_{U_i}$. At any point $x \in U_i$, the velocity vector will be normal to the level set of φ containing x, will point towards the center of curvature in the tangent space $T_M(x)$, and will have length $F(\kappa_g)$.

The geodesic curvature of the curve $\varphi^{-1}(C)$ in terms of φ is

$$\kappa_g = \frac{(N \times \tau)\cdot n}{1-(n\cdot N)^2}\left(\tau\cdot\left(\left(\frac{n\cdot N}{\|\nabla f\|}\nabla^2 f - \frac{1}{\|\nabla\varphi\|}\nabla^2\varphi\right)\tau\right)\right),$$

where $n = \nabla\varphi/\|\nabla\varphi\|$, $N = \nabla f/\|\nabla f\|$, and

$$\tau = \frac{\nabla f \times \nabla\varphi}{\|\nabla f \times \nabla\varphi\|}.$$

The direction of the velocity vector is the same as the orthogonal projection of $\nabla\varphi$ onto T_M, so

$$v = \tau \times N = \frac{n-(n\cdot N)N}{\|n-(n\cdot N)N\|}$$

and the velocity at x on M is described by

$$\dot{x}\cdot v = F(\kappa_g).$$

The computing is done on the sets $\pi_i(U_i)$, so we want the equation of motion in terms of Φ_i. For a point $x \in \pi_i(U_i)$, we have

$$\dot{x}\cdot\eta = F(\kappa_g)D\pi_i(v)\cdot\eta,$$

where $\eta = \nabla\Phi_i/\|\nabla\Phi_i\|$ is the unit normal to the level set containing $\Phi_i(x)$. Setting

$$\tilde{F}(\kappa_g) = F(\kappa_g)D\pi_i(v)\cdot\nabla\Phi_i/\|\nabla\Phi_i\|,$$

the equation of motion in terms of Φ_i is given by

$$0 = (\Phi_i)_t + \tilde{F}(\kappa_g)\|\nabla\Phi_i\|. \tag{6.1}$$

6.2. Geodesic Curvature Algorithm

Putting everything together, the general algorithm for curvature flow on a manifold can be stated as follows:

1. Choose coordinate patches and maps to represent the manifold M.
2. Initialize the functions Φ_i on each coordinate patch.
3. Compute the boundary values in each coordinate patch based on overlap values with neighboring patches.
4. Advance each Φ_i in time according to (6.1).
5. Go to step 3.

For any t, the curve $\gamma(t)$ can be reconstructed from

$$\gamma(t) = \bigcup \pi_i^{-1}(\Phi_i^{-1}(0,t)) \tag{6.2}$$

We now discuss the details of each of these steps.

Given a manifold M, it is important to choose simply connected coordinate patches $\{U_i, \pi_i\}$, so that any simple curve can be represented by a level set of a function φ on U_i. The equations given above are for the case when π_i maps onto a rectangular coordinate system in $\mathbb{R}^2$. In the overlap sets, where $U_i \cap U_j \neq \varnothing$, there must be at least three grid points in the overlap between $V_i = \pi_i(U_i)$ and $V_j - \pi_j(U_j)$. The computation of the boundary conditions for each V_i is made easier if the grid points and projection maps π_i are chosen so that grid points are compatible, that is, if $x \in V_i$ is a grid point in V_i and $\pi_i^{-1}(x) \in U_i \cap U_j$, then $\pi_j(\pi_i^{-1}(x))$ is also a grid point in V_j.

For example, let M be a torus of revolution with large radius R and small radius r symmetric about the z-axis. One choice of coordinate patches is shown in Figure 18: in symbols,

$$U_1 = \{(x,y,z) : \sqrt{x^2+y^2} > R-\varepsilon, x > -\varepsilon\},$$

$$U_2 = \{(x,y,z) : \sqrt{x^2+y^2} < R+\varepsilon, x > -\varepsilon\},$$

$$U_3 = \{(x,y,z) : \sqrt{x^2+y^2} < R-\varepsilon, x < \varepsilon\},$$

$$U_4 = \{(x,y,z) : \sqrt{x^2+y^2} > R-\varepsilon, x < \varepsilon\},$$

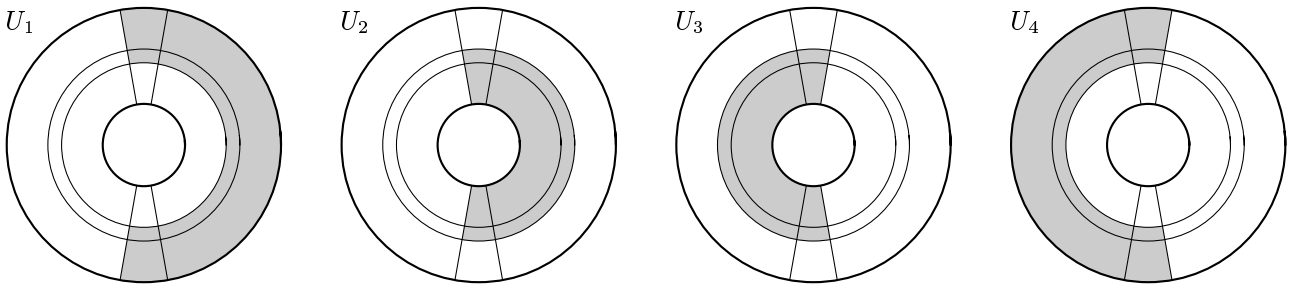

FIGURE 18. Example of coordinate patches on a torus.

where each π_i maps U_i to

$$V_i = \left(-\frac{\pi}{2} - \varepsilon, \frac{\pi}{2} + \varepsilon\right) \times \left(-\frac{\pi}{2} - \varepsilon, \frac{\pi}{2} + \varepsilon\right)$$

in the natural way. Then a uniform rectangular grid is placed on the closure of V_i.

The objective when initializing the functions Φ_i is to satisfy (6.2). We use the signed distance function, where the distance is computed on the manifold. The sign of Φ_i is assigned on each coordinate patch independently; thus

$$|\Phi_i(\pi_i(x))| = |\Phi_j(\pi_j(x))|$$

at each grid point $x \in U_i \cap U_j$. This is important for ensuring consistent motion in the overlap regions. If F is not an odd function, we must additionally require that $\Phi_i(\pi_i(x)) = \Phi_j(\pi_j(x))$.

The evolution on each patch V_i is computed on the interior grid points of V_i. The values at the boundary are taken from neighboring patches. Let x be a grid point on the boundary of V_i. By construction, $\pi_i^{-1}(x)$ is in the interior of some other patch U_j. Therefore $\Phi_i(x) = \pm\Phi_j(\pi_j(\pi_i^{-1}(x)))$, where the sign is positive if $\Phi_i \circ \pi_i$ and $\Phi_j \circ \pi_j$ have same sign in the interior of $U_i \cap U_j$, and negative otherwise.

The overlap of two coordinate patches may be disconnected. The sign convention must be determined individually for each connected component. For example, the two outer patches in Figure 18 overlap in two components. It is possible for both patches to share the same sign convention in one overlap while having the opposite convention in the other overlap. This property makes it possible to model a single curve on a torus as a level set of a function within each coordinate patch.

Following the argument in Section 5.1, we break F into constant and nonconstant parts, $F(\kappa) = F_1 - F_2(\kappa)$. Equation (6.1) then becomes

$$\Phi_{it} + \tilde{F}_1\|\nabla\Phi_i\| = \tilde{F}_2(\kappa_g)\|\nabla\Phi_i\|.$$

As in section 2, upwind techniques from hyperbolic conservation laws are used to compute the left-hand side and central differences are used on the right-hand side.

6.3. Examples

We begin with flow on a sphere. The sphere is constructed with a single coordinate patch parametrized by spherical coordinates. The gap in Figure 19 shows the boundary of the coordinate patch. The picture on the left shows an initial circle just smaller than a great circle shrinking to a point at the top. The one on the right shows a periodic curve, symmetric with respect to the equator, collapsing to the equator.

Next, we show flow on a torus. If the torus is constructed with a single coordinate patch, then it is not possible to model a single noncontractible curve using a level set approach. For curves which are not too complicated, it is possible to construct a second curve to allow for the level set formulation. In figure 20, a single coordinate patch is used and the flow of two nonintersecting curves is computed.

However, if multiple coordinate patches are used, a required sign change can be handled by the communications between patches. We can then model

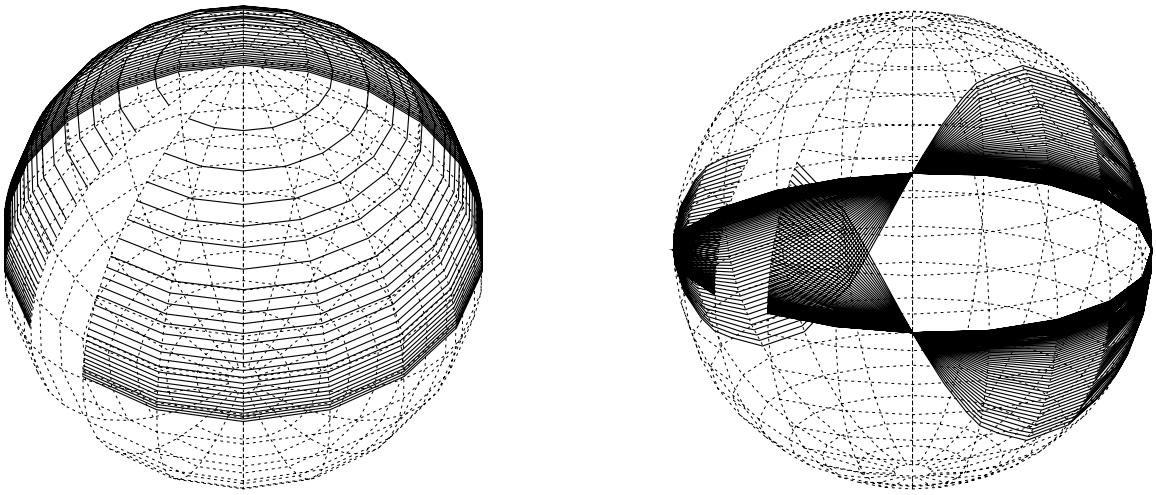

FIGURE 19. Curves evolving on a sphere under the action of geodesic curvature. Left: a circle (other than a great circle) shrinks to a point. Right: a periodic curve symmetric with respect to the equator converges to the equator.

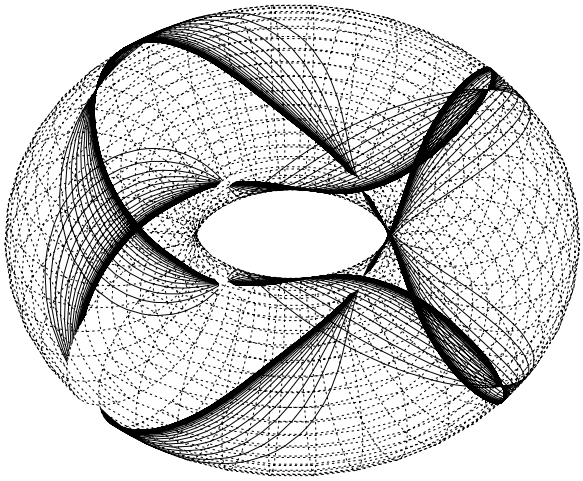

FIGURE 20. Two curves, forming the zero set of a function on a torus parametrized by a single rectangular patch, flow under geodesic curvature.

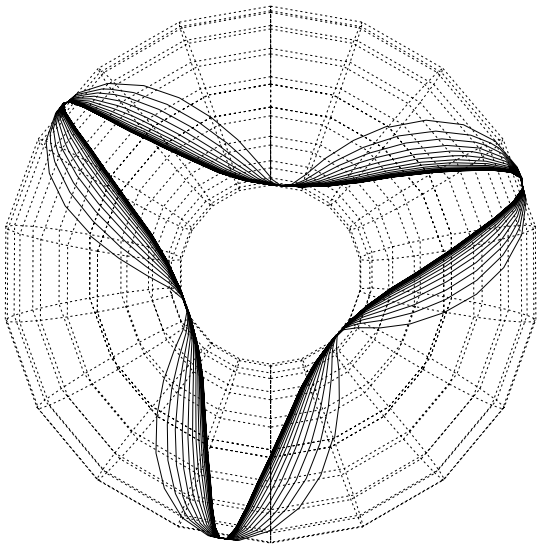

FIGURE 21. A single curve flows under geodesic curve on a torus parametrized by four rectangular patches.

a single curve on a torus. Figure 21 shows such a curve. The coordinate patches are those of Figure 18.

Subsets of manifolds can also be used. Figure 22 shows two curves flowing on a helicoid. Another example is when the submanifold is the graph of a function $f : \mathbb{R}^2 \to \mathbb{R}$. In Figure 23 we use $f(x, y) = 2\cos(2\sqrt{x^2 + y^2})$.

Finally, we show several flows on a cube. The cube has one coordinate patch for each face. The first experiment involves comparing the flow on a cube with sharp edges to the flow on one with increasingly smoother edges: see Figure 24. The initial curve is flatter on the front faces than on the top. We see that the flow is similar in all cases, with the curve collapsing to a point near the corner. Two other flows on a cube are shown in Figure 25.

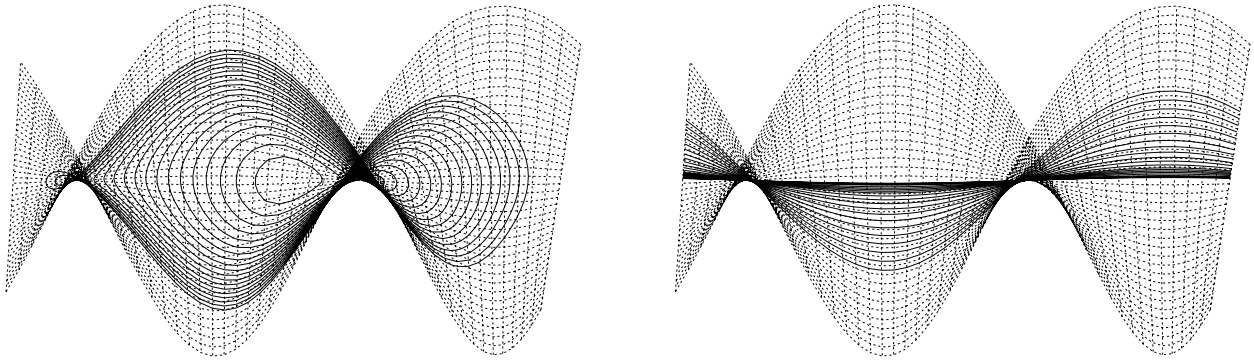

FIGURE 22. Curves evolving under geodesic curvature on a helicoid. Left: an oval shrinks to a point. Right: a periodic curve flowing towards the central axis of the helicoid. Boundary conditions are periodic right and left: one-sided derivatives on the sides of a single rectangular coordinate patch.

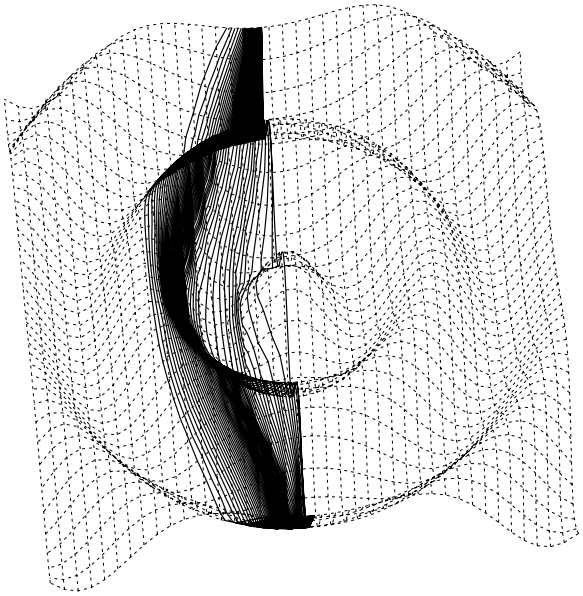

FIGURE 23. On the graph of $2\cos(2\sqrt{x^2+y^2})$, a straight line slightly off-center flows away from the center over a ridge. One-sided derivatives are used for all boundaries.

ACKNOWLEDGEMENTS

All calculations were performed at the University of California at Berkeley and the Lawrence Berkeley Laboratory (LBL). The figures were computed using the facilities of the Graphics Group at LBL.

We would like to thank L. Craig Evans, F. A. Grünbaum, Ole Hald, and V. Oliker for helpful discussions.

NOTE

A video (VHS format) of the evolving surfaces is available from the second author.

REFERENCES

[Brakke 1978] K. A. Brakke, *The Motion of a Surface by Its Mean Curvature*, Princeton University Press, Princeton, New Jersey, 1978.

[Brakke 1992] K. A. Brakke, "The Surface Evolver", *Experimental Mathematics* **1** (1992), 141–165.

[Chen et al. 1991] Y. Chen, Y. Giga, and S. Goto, "Uniqueness and existence of viscosity solutions of generalized mean curvature flow equations", *J. Diff. Geom.* **33** (1991), 749–786.

[Chopp 1992] D. L. Chopp, "Flow under geodesic curvature", Technical Report CAM 92-23, UCLA, May 1992.

[Chopp 1993] D. L. Chopp, "Computing minimal surfaces via level set curvature flow", *J. Comp. Phys.*, **106** (May 1993), 77–91.

[Crandall and Lions 1983] M. G. Crandall and P. L. Lions, "Viscosity solutions of Hamilton–Jacobi equations", *Trans. Amer. Math. Soc.* **277** (1983), 1–42.

[Evans et al. 1992] L. C. Evans, H. M. Soner, and P. E. Souganidis, "Phase transitions and generalized motion by mean curvature", *Comm. Pure Appl. Math.* **45** (1992), 1097–1123.

[Evans and Spruck 1991] L. C. Evans and J. Spruck, "Motion of level sets by mean curvature I", *J. Diff. Geom.* **33** (1991), 635–681.

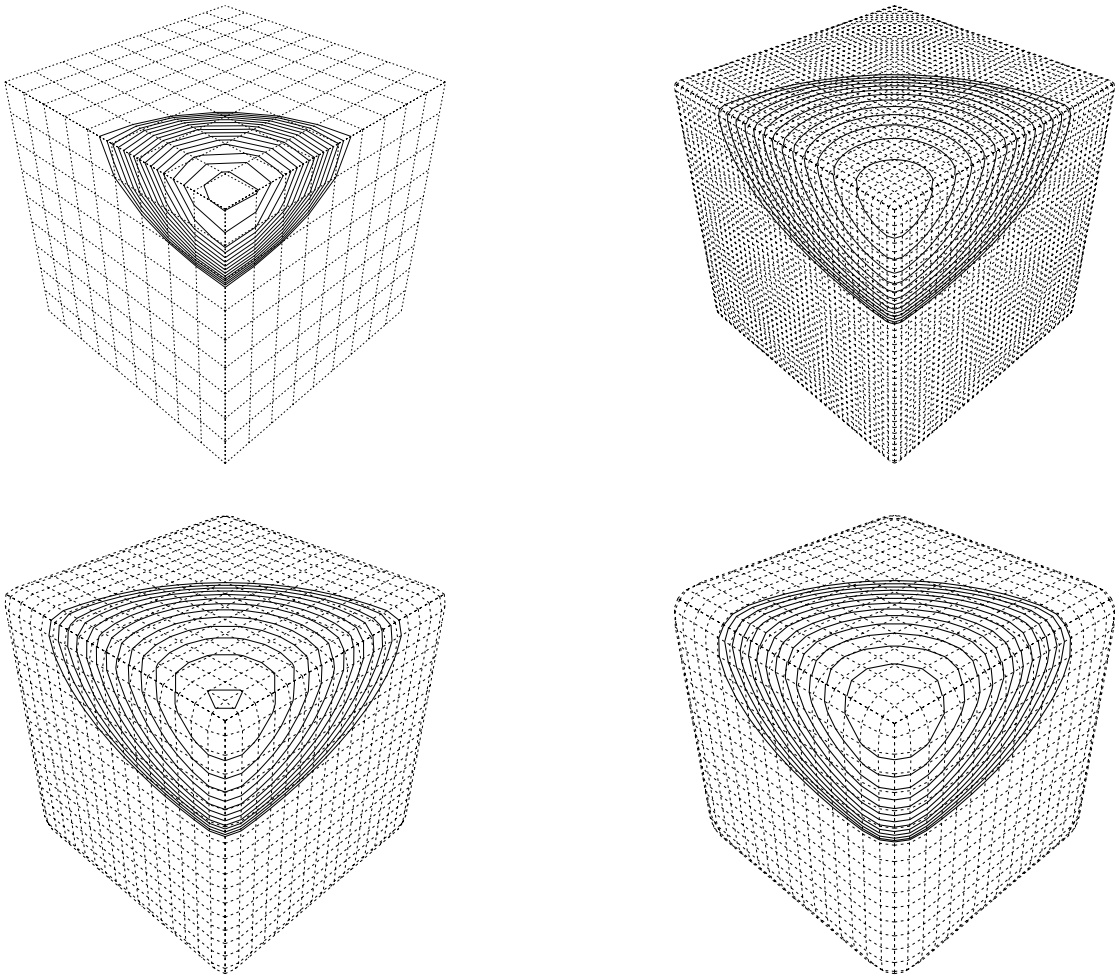

FIGURE 24. The same loop flows on a cube with sharp edges (top left), then on cubes with increasingly rounded edges.

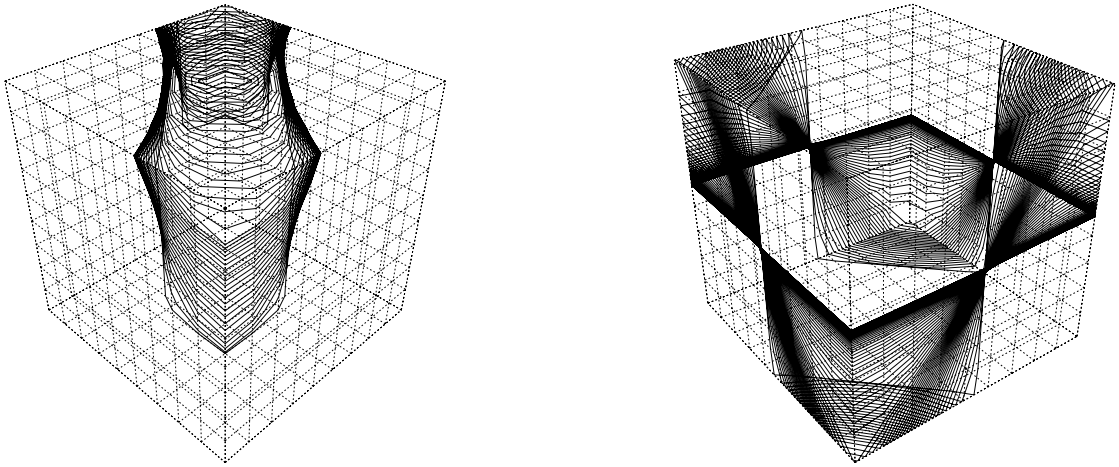

FIGURE 25. Left: a loop is pulled over two opposite corners on a face of a cube. Right: another loop is pulled over alternating corners.

[Evans and Spruck 1991] L. C. Evans and J. Spruck, "Motion of level sets by mean curvature II", *Trans. Amer. Math. Soc.* **330** (1992), 321–332.

[Falcone et al. 1990] M. Falcone, T. Giorgi, and P. Loretti, "Level sets of viscosity solutions and applications", Technical report, Istituto per le Applicazioni del Calcolo, Rome, 1990.

[Gage 1983] M. Gage, "An isoperimetric inequality with applications to curve shortening", *Duke Math. J.* **50** (1983), 1225–1229.

[Gage 1984] M. Gage, "Curve shortening makes convex curves circular", *Inventiones Math.*, **76** (1984), 357–364.

[Gage and Hamilton 1986] M. Gage and R. S. Hamilton, "The equation shrinking convex planes curves", *J. Diff. Geom.* **23** (1986), 69–96.

[Giga and Goto 1992] Y. Giga and S. Goto, "Motion of hypersurfaces and geometric equations", *J. Math. Soc. Japan* **44** (1992), 99–111.

[Grayson 1987] M. Grayson, "The heat equation shrinks embedded plane curves to round points", *J. Diff. Geom.* **26** (1987), 285–314.

[Grayson 1989] M. Grayson, "A short note on the evolution of surfaces via mean curvature", *Duke Math. J.* **58** (1989), 555–558.

[Hicks 1965] N. J. Hicks, *Notes on Differential Geometry*, Van Nostrand, Princeton, NJ, 1965.

[Huisken 1984] G. Huisken, "Flow by mean curvature of convex surfaces into spheres", *J. Diff. Geom.* **20** (1984), 237–266.

[Mulder et al. 1992] W. Mulder, S. Osher, and J. A. Sethian, "Computing interface motion in compressible gas dynamics", *J. Comp. Phys.*, **100** (May 1992), 209–228.

[Oliker 1991] V. Oliker, "Evolution of nonparametric surfaces with speed depending on curvature, I: The Gauss curvature case", *Indiana Univ. Math. J.* **40** (1991), 237–258.

[Osher and Sethian 1988] S. Osher and J. A. Sethian, "Fronts propagating with curvature-dependent speed: Algorithms based on Hamilton–Jacobi formulations", *J. Comp. Phys.* **79** (1988), 12–49.

[Sethian 1985] J. A. Sethian, "Curvature and the evolution of fronts", *Comm. Math. Phys.* **101** (1985), 487–499.

[Sethian 1987] J. A. Sethian, "Numerical methods for propagating fronts", pp. 155–164 in *Variational Methods for Free Surface Interfaces* (edited by P. Concus and R. Finn), Springer, New York, 1987.

[Sethian 1989] J. A. Sethian, "A review of recent numerical algorithms for hypersurfaces moving with curvature-dependent speed", *J. Diff. Geom.* **31** (1989), 131–161.

[Sethian and Chopp 1992] J. A. Sethian and D. L. Chopp, "Flow under mean curvature: Singularity formation and minimal surfaces", in *Computational Crystal Growers Workshop* (video and booklet, edited by J. E. Taylor), American Mathematical Society, Providence, RI, 1992.

[Sethian and Strain 1992] J. A. Sethian and J. Strain, "Crystal growth and dendrite solidification", *J. Comp. Phys.* **98** (1992), 231–253.

[Zhu and Sethian 1992] J. Zhu and J. A. Sethian, "Projection methods coupled to level set interface techniques", *J. Comp. Phys.* **102** (1992), 128–138.

David L. Chopp, University of Washington, Department of Mathematics, GN-50, Seattle, WA 98115
(chopp@math.washington.edu)

James A. Sethian, Department of Mathematics, University of California, Berkeley, CA 94720
(sethian@math.berkeley.edu)

Received July 21, 1993; accepted in revised form January 17, 1994